Postprint of: Mul M., de la Rubia V., Fotyga G., Lamęcki A., Mrozowski M.: Regularized Local Multivariate Reduced-Order Models With Nonaffine Parameter Dependence, IEEE TRANSACTIONS ON MICROWAVE THEORY AND TECHNIQUES, Vol. 67, iss. 5 (2019), pp. 1778-1789, DOI: 10.1109/TMTT.2019.2906303

Regularized Local Multivariate Reduced-Order Models with Nonaffine Parameter Dependence

Martyna Mul, Valentín de la Rubia, Grzegorz Fotyga, Adam Lamecki, *Senior Member, IEEE* and Michal Mrozowski, *Fellow, IEEE*

***Abstract*—This paper addresses a singular problem, not yet discussed in the literature, which occurs when parametric reduced-order models are created using a subspace projection approach with multiple concatenated projection bases. We show that this technique may lead to the appearance of localized artifacts in the frequency characteristics of a system, even when the reduced-order projection basis is rich enough to describe the original system. These artifacts are found to be related to nonphysical poles of the transfer function that emerge whenever more than one projection basis is used, each spanning a similar space, and these bases are directly put together to build multivariate reduced-order models. These unwanted poles are identified using the Bauer–Fike theorem and then the parametrized reduced-order model is regularized with a simple deflation procedure that completely removes the artifacts due to nonphysical resonances from the circuit characteristics. Finally, real-life numerical examples illustrate the accuracy and abilities of the proposed approach.**

***Index Terms*—Computer-aided engineering, design automation, finite-element method (FEM), parametric model order reduction, parametric macromodels.**

I. Introduction

THE finite-element and finite-difference methods are among the most accurate and versatile numerical approaches for solving Maxwell's equations. These methods underpin the software tools used to design passive microwave components and antennas. The accuracy of this numerical analysis comes at the price of its relatively high computational cost: these techniques, when used for time-harmonic fields, involve solving a large sparse system of equations. This cost may be significantly reduced when we are interested in the circuit behavior within a certain frequency band. To this end, various fast-frequency sweep techniques can be applied. In this context, subspace-projection-type model order reduction (MORe) algorithms should be mentioned. In these algorithms, the original large sparse system of equations is converted to a small dense linear algebra problem by applying the Galerkin method with an orthogonal set of vectors, giving rise to basis and testing spaces. The vectors spanning the subspace in which the solution is sought can be found by means of, for example, the reduced-basis method [1] or by moment-matching MORe algorithms [2]. The projection basis can be established for the entire computational domain—we will refer to this variant as global MORe [1], [3]–[9], or the domain can be divided into subregions and a separate basis can then be determined for each subregion—we will refer to this other variant as local MORe [7], [8], [10]–[15]. The reduction can be performed hierarchically [16], [17] to even further reduce the size of the final problem. The small system resulting from the Galerkin projection can be solved with very little effort for a large number of frequency points. The actual solution can then be found as a linear combination of the basis vectors with frequency-dependent weights provided by solving the reduced-order system. MORe provides an approximate solution in the frequency band of interest, but the accuracy can be increased and the bandwidth extender by adding new vectors to the basis. To control this process, error estimators [1], [4], [18]–[22] can be employed.

Fast-frequency sweep MORe algorithms can be regarded as a way to accelerate the parametric analysis of a system of partial differential equations with frequency as a parameter. It should be noted that, in practice, frequency is not the only parameter that can change. In microwave circuit design and optimization problems, in yield analysis, and in parametric studies, it is necessary to repeat full-wave simulations for a variety of different geometries. Since this process is very time-consuming, it is tempting to develop MORe techniques that take into account other variables beside frequency. This leads to the problem known as parametric model order reduction (PMORe). It should be noted that PMORe is more demanding, since the original system parameter dependency is nonlinear and not affine, in general, as it is the case in fast-frequency sweep MORe.

Several approaches have been proposed for the PMORe problem. Publication [23] gives an excellent overview of state-of-the-art projection-based methods in parametric dynamical systems with a discussion of advantages and disadvantages for each methodology. Based on [23], it can be stated that there are three main categories of projection-based techniques. One category constructs a single projection basis for the entire parameter space, while a second category involves multiple bases constructed for many points in the design space and requires some sort of interpolation technique—either at the projection basis level, the reduced-order transfer function level, or the reduced-order model matrices. It should be noted that

M. Mul, G. Fotyga, A. Lamecki and M. Mrozowski are with the Faculty of Electronics, Telecommunications, and Informatics, Gdańsk University of Technology, Poland (e-mail: martyna.czarniewska@pg.edu.pl, grzfotyg@pg.gda.pl, adam.lamecki@ieee.org, m.mrozowski@ieee.org).

V. de la Rubia is with the Departamento de Matemática Aplicada a las TIC, ETSI de Telecomunicación, Universidad Politécnica de Madrid, 28040 Madrid, Spain (e-mail: valentin.delarubia@upm.es).

This work was supported by the Foundation for Polish Science within the TEAM-TECH program, cofinanced by the European Regional Development Fund, Smart Growth Operational Program 2014-2020 (project EDISOn: Electromagnetic Design of flexIble SensOrs), and by the Polish National Science Centre under contract UMO-2013/09/B/ST7/04202.

in the first category, a single basis is formed by concatenating the individual bases obtained for several parameter samples and no interpolation is needed. Finally, the third category is a straightforward extension of the reduced-basis method to the multidimensional parameter case, but this approach is computationally valid only if an affine parameter decomposition can be applied and the number of parameters is small. All three approaches have been used in the context of computer simulations of microwave components and antennas [24]–[30].

Taking into account geometry as a parameter, which is of paramount importance in computer-aided design problems, the mesh deformation technique [31] makes PMORe straightforward, since the same mesh topology is preserved along the mesh morphing as the geometry parameter changes. Indeed, in this scenario, the approach based on concatenated bases is particularly simple to implement in FEM and makes it straightforward to handle nonaffine geometry parameter dependence [32], [33]. Each time a new device geometry is analyzed, the field solution is guaranteed to be represented within the *same* FEM basis. This overcomes the difficulty in managing different representation basis for each new geometry in the circuit to be designed. However, our studies have shown that, as new sets of vectors from new parameter samples are appended and the basis is augmented, the reduced-order system shows additional nonphysical poles which may affect the response of the circuit in the frequency band of interest. These additional poles occur in both global and local PMORe schemes. To the best of our knowledge, neither this phenomenon nor methods of dealing with these nonphysical poles have been discussed to date.

In this paper, we address the problem of these additional false poles in the context of local parametrized reduced-order models (PROMs) in the finite-element method obtained using concatenated projection bases and geared towards multivariate models with nonaffine parameter dependence. We show that these poles are related to nonphysical localized resonances of the subregions subjected to MORe and emerge whenever more than one projection basis is used to build multivariate reduced-order models. When the local PROMs are substituted back into the original system, the original circuit response is modified accordingly. Because of the presence of additional poles in these local PROMs, the circuit response for the entire structure may be affected. This results in the presence of artifacts in the circuit response in the form of spikes. As a consequence, the PROM is completely useless since the actual circuit behavior can not be identified in this setting. To avoid this problem, we investigate ways of identifying these nonphysical local resonances very early on when a local PROM is generated, in order to distinguish them from true resonances and ultimately to eliminate nonphysical poles with little computational effort from the final system of FEM equations for the entire structure. As a result, high-quality regularized local PROMs are obtained and the response of the whole circuit is completely free of spikes. This gives rise to a reliable parametric MORe process.

This paper is organized as follows. In Section II we review the methodology of constructing local multivariate reduced-order models from FEM equations based on concatenated local projection bases. Section III discusses the problem of localized artifacts. i.e. spikes, that appear in the circuit characteristics and identifies their source. In Section IV we propose two techniques for regularizing the local PROMs. i.e. removing the spikes. Section V shows numerical examples and illustrates the capabilities of the proposed approach as well as its accuracy. We show that a complete elimination of the artifacts can easily be achieved by applying the Bauer-Fike theorem to the poles of the transfer function of a PROM. Finally, in Section VI, we comment on the conclusions.

II. Local Parametrized Reduced-Order Models

An efficient technique based on MORe for fast parametric FEM analysis of microwave components involving several parameters by means of local PROMs has been addressed in [34]. In this methodology, the analysis domain is divided into subregions. For each subregion, different local projection subbases, namely, $\mathbf{Q}_j,\ j = 1, \ldots, M$—each one standing for the characteristics of the subregion in the M parameter samples, are computed and concatenated to create a single local projection basis. The subbases for all subdomains are found at sample points within the parameter space $\mathcal{P}$, where all different parametric variables are taken into account. Whenever geometry variables are considered, the mesh deformation technique [31] is applied locally, in each subregion, in order to be able to describe the field solutions within the *same* representation FEM basis for each sample in the parameter space $\mathcal{P}$. As a result, not only is the number of degrees of freedom and the topology of the mesh kept constant in the parameter-dependent problem, but also the concatenation of subbases is enabled in a straightforward way, allowing for PMORe where geometry dependency is taken into account. In the same token, the process of uplifting local bases is controlled by local and global goal-oriented error estimators [19], [35]. These estimators also serve as indicators to determine the quality of the PROMs. Once a suitable basis is found, a local PROM is formed and substituted back into the original system of FEM equations in order to solve for the whole computational domain.

Let us provide some details of the finite-element formulation that are essential to understand the proposed MORe procedure. Further information can be found in [13], [17], [34], [36]. Finite-element discretization of the time-harmonic Maxwell's equations leads to an n-dimensional linear system of the form:

$$\begin{aligned} \left(\mathbf{\Gamma} + s^2\mathbf{C}\right)\mathbf{E} &= s\mathbf{B}\mathbf{I} \\ \mathbf{U} &= \mathbf{B}^T\mathbf{E}, \end{aligned} \tag{1}$$

with $\mathbf{\Gamma}, \mathbf{C} \in \mathbb{C}^{n\times n}$ being the stiffness and mass FEM sparse matrices, respectively, $s = jk_0$ is a normalized complex frequency, where k_0 is the wavenumber. $\mathbf{B} \in \mathbb{C}^{n\times m}$ is a matrix operator mapping the coupling of the excitation currents at the ports to the electric fields on the analysis domain. $\mathbf{E} \in \mathbb{C}^{n\times m}$ is the matrix of unknown coefficients associated with the FEM basis functions representing the electric field, where m is the number of excitation vectors. $\mathbf{I}$ and $\mathbf{U}$ contain m amplitudes of the current and voltage waves of the modes at the ports, respectively. We assume for simplicity that the structure is excited by m modes with one mode at each port.

The entries of the stiffness and mass FEM matrices change as we explore the design parameter space $\mathcal{P}$. Let us use $\mathbf{p}$ to represent the vector of variables—either geometric or material parameters, that are allowed to change in the parameter space $\mathcal{P}$. Equation (1) can then be represented as a parameter-dependent system, thus:

$$\begin{aligned}\left(\mathbf{\Gamma}(\mathbf{p}) + s^2\mathbf{C}(\mathbf{p})\right)\mathbf{E}(s,\mathbf{p}) &= s\mathbf{B}\mathbf{I}\\ \mathbf{U} &= \mathbf{B}^T\mathbf{E}(s,\mathbf{p}).\end{aligned} \tag{2}$$

Solving for the electric field in the above problem, we can obtain the impedance matrix $\mathbf{Z}$ describing the circuit, viz.,

$$\begin{aligned}\mathbf{U} &= \mathbf{Z}\mathbf{I}\\ \mathbf{Z}(s,\mathbf{p}) &= \mathbf{B}^T\left(\mathbf{\Gamma}(\mathbf{p}) + s^2\mathbf{C}(\mathbf{p})\right)^{-1}\mathbf{B}.\end{aligned} \tag{3}$$

Let us point out that the admittance matrix $\mathbf{Y}$ of the circuit is the inverse mapping between current and voltage waves, namely, $\mathbf{I} = \mathbf{Y}\mathbf{U}$.

In order to be able to rapidly solve the system of FEM equations, the analysis domain Ω is partitioned into different nonoverlapping interior subdomains which are of special interest for parametric study, namely, $\Omega_j, j = 1,\ldots,J$, and the complement in Ω, namely, subdomain Ω_0. These interior nonoverlapping subdomains define artificial boundaries within the analysis domain Ω, viz., $\partial\Omega_j, j = 1,\ldots,J$. In this setting, we would like to highlight the partition structure in the system of FEM equations (1). The degrees of freedom in the electric field $\mathbf{E}$ are decomposed into port unknowns $\mathbf{E}_P$, artificial boundary unknowns $\mathbf{E}_{\partial\Omega}$, and subdomain unknowns $\mathbf{E}_\Omega$, where $\mathbf{E}_\Omega^T = \left[\mathbf{E}_{\Omega_0}^T\ \mathbf{E}_{\Omega_1}^T\ldots\ \mathbf{E}_{\Omega_J}^T\right]$. As a result, the electric field $\mathbf{E}$ in (1) can be written as $\mathbf{E}^T = \left[\mathbf{E}_P^T\ \mathbf{E}_{\partial\Omega}^T\ \mathbf{E}_\Omega^T\right]$, giving rise to the following partition structure in the FEM system matrices in (1):

$$\begin{aligned}\mathbf{\Gamma} &= \begin{bmatrix}\mathbf{\Gamma}_P & 0 & \mathbf{G}_{\Omega P}^T\\ 0 & \mathbf{\Gamma}_{\partial\Omega} & \mathbf{G}_{\Omega\delta}^T\\ \mathbf{G}_{\Omega P} & \mathbf{G}_{\Omega\delta} & \mathbf{\Gamma}_\Omega\end{bmatrix}\\ \mathbf{C} &= \begin{bmatrix}\mathbf{C}_P & 0 & \mathbf{T}_{\Omega P}^T\\ 0 & \mathbf{C}_{\partial\Omega} & \mathbf{T}_{\Omega\delta}^T\\ \mathbf{T}_{\Omega P} & \mathbf{T}_{\Omega\delta} & \mathbf{C}_\Omega\end{bmatrix}\\ \mathbf{B}^T &= \begin{bmatrix}\mathbf{B}_P^T & 0 & 0\end{bmatrix},\end{aligned} \tag{4}$$

where $\mathbf{G}_{\Omega P}$, $\mathbf{T}_{\Omega P}$ and $\mathbf{G}_{\Omega\delta}$, $\mathbf{T}_{\Omega\delta}$ denote the blocks in the FEM matrices that couple the ports P to subregions Ω_j, and the artificial boundaries $\partial\Omega_i$ to subregions Ω_j, respectively. It should be noted that the excitation coupling $\mathbf{B}_P$ is only applied at the ports P. Matrices $\mathbf{\Gamma}_\Omega$ and $\mathbf{C}_\Omega$ are block-diagonal, i.e., $\mathbf{\Gamma}_\Omega = \mathrm{diag}[\mathbf{\Gamma}_{\Omega_j}], \mathbf{C}_\Omega = \mathrm{diag}[\mathbf{C}_{\Omega_j}], j = 0,1,\ldots,J$, whereas the FEM matrices coupling different blocks have the following structure:

$$\begin{aligned}\mathbf{G}_{\Omega P}^T &= \begin{bmatrix}\mathbf{G}_{\Omega_0 P}^T & \mathbf{G}_{\Omega_1 P}^T & \ldots & \mathbf{G}_{\Omega_J P}^T\end{bmatrix}\\ \mathbf{G}_{\Omega\delta}^T &= \begin{bmatrix}\mathbf{G}_{\Omega_0\delta}^T & \mathbf{G}_{\Omega_1\delta}^T & \ldots & \mathbf{G}_{\Omega_J\delta}^T\end{bmatrix}\end{aligned} \tag{5}$$

and

$$\begin{aligned}\mathbf{T}_{\Omega P}^T &= \begin{bmatrix}\mathbf{T}_{\Omega_0 P}^T & \mathbf{T}_{\Omega_1 P}^T & \ldots & \mathbf{T}_{\Omega_J P}^T\end{bmatrix}\\ \mathbf{T}_{\Omega\delta}^T &= \begin{bmatrix}\mathbf{T}_{\Omega_0\delta}^T & \mathbf{T}_{\Omega_1\delta}^T & \ldots & \mathbf{T}_{\Omega_J\delta}^T\end{bmatrix}.\end{aligned} \tag{6}$$

A. Local Transfer Function, its Poles, and Local Parametrized Reduced-Order Model

In order to apply MORe locally in a specific subregion, we first define a transfer function associated with this subregion. For the sake of simplicity, let us consider an analysis domain Ω where a single subregion Ω_1 is taken into account for parametric MORe. As a result, the artificial boundary $\partial\Omega_1$ divides the original analysis domain Ω into two subdomains, namely, Ω_0 and Ω_1. This is the simplest case but it can easily be generalized for multiple subdomains. In this framework, the electric field $\mathbf{E}$ in (1) can be written as $\mathbf{E}^T = \left[\mathbf{E}_P^T\ \mathbf{E}_{\partial\Omega_1}^T\ \mathbf{E}_{\Omega_0}^T\ \mathbf{E}_{\Omega_1}^T\right]$, giving rise to the following structure in the FEM system matrices in (1):

$$\begin{aligned}\mathbf{\Gamma} &= \begin{bmatrix}\mathbf{\Gamma}_P & 0 & \mathbf{G}_{\Omega_0 P}^T & \mathbf{G}_{\Omega_1 P}^T\\ 0 & \mathbf{\Gamma}_{\partial\Omega_1} & \mathbf{G}_{\Omega_0\delta}^T & \mathbf{G}_{\Omega_1\delta}^T\\ \mathbf{G}_{\Omega_0 P} & \mathbf{G}_{\Omega_0\delta} & \mathbf{\Gamma}_{\Omega_0} & 0\\ \mathbf{G}_{\Omega_1 P} & \mathbf{G}_{\Omega_1\delta} & 0 & \mathbf{\Gamma}_{\Omega_1}\end{bmatrix}\\ \mathbf{C} &= \begin{bmatrix}\mathbf{C}_P & 0 & \mathbf{T}_{\Omega_0 P}^T & \mathbf{T}_{\Omega_1 P}^T\\ 0 & \mathbf{C}_{\partial\Omega_1} & \mathbf{T}_{\Omega_0\delta}^T & \mathbf{T}_{\Omega_1\delta}^T\\ \mathbf{T}_{\Omega_0 P} & \mathbf{T}_{\Omega_0\delta} & \mathbf{C}_{\Omega_0} & 0\\ \mathbf{T}_{\Omega_1 P} & \mathbf{T}_{\Omega_1\delta} & 0 & \mathbf{C}_{\Omega_1}\end{bmatrix}\\ \mathbf{B}^T &= \begin{bmatrix}\mathbf{B}_P^T & 0 & 0 & 0\end{bmatrix}.\end{aligned} \tag{7}$$

As a result of this structure in (1), we can explicitly write down the following local system of equations, thus:

$$\begin{aligned}0\cdot\mathbf{E}_P + \mathbf{A}_{\partial\Omega_1}(s)\mathbf{E}_{\partial\Omega_1} + \mathbf{F}_{\Omega_0\delta}^T(s)\mathbf{E}_{\Omega_0} + \mathbf{F}_{\Omega_1\delta}^T(s)\mathbf{E}_{\Omega_1} &= s\cdot 0\cdot\mathbf{I}\\ \mathbf{F}_{\Omega_1 P}(s)\mathbf{E}_P + \mathbf{F}_{\Omega_1\delta}(s)\mathbf{E}_{\partial\Omega_1} + 0\cdot\mathbf{E}_{\Omega_0} + \mathbf{A}_{\Omega_1}(s)\mathbf{E}_{\Omega_1} &= s\cdot 0\cdot\mathbf{I},\end{aligned} \tag{8}$$

where $\mathbf{A}_\omega(s) = \mathbf{\Gamma}_\omega + s^2\mathbf{C}_\omega$ and $\mathbf{F}_\omega(s) = \mathbf{G}_\omega + s^2\mathbf{T}_\omega$, and subscript ω is used to represent suitable indices related to subregions, ports or boundaries in the above equation.

It should be noted that subregion Ω_1 is not directly coupled to the ports P and, as a result, $\mathbf{F}_{\Omega_1 P}(s) = 0$. In the end, (8) simplifies to the following relation:

$$\mathbf{A}_{\partial\Omega_1}(s)\mathbf{E}_{\partial\Omega_1} + \mathbf{F}_{\Omega_0\delta}^T(s)\mathbf{E}_{\Omega_0} + \mathbf{F}_{\Omega_1\delta}^T(s)\mathbf{E}_{\Omega_1} = 0 \tag{9a}$$

$$\mathbf{F}_{\Omega_1\delta}(s)\mathbf{E}_{\partial\Omega_1} + \mathbf{A}_{\Omega_1}(s)\mathbf{E}_{\Omega_1} = 0. \tag{9b}$$

Recall that $\mathbf{A}_{\Omega_1}(s) = \mathbf{\Gamma}_{\Omega_1} + s^2\mathbf{C}_{\Omega_1}$. Equation (9b) shows that the eigenvalues of the matrix pencil $(\mathbf{\Gamma}_{\Omega_1}, \mathbf{C}_{\Omega_1})$ represent the eigenresonances in the perfect electric conductor (PEC) cavity Ω_1, whose PEC wall is formed by the artificial boundary $\partial\Omega_1$. In the same token, these eigenresonances are the poles of the admittance matrix describing the electromagnetics in subdomain Ω_1.

Solving for the electric field $\mathbf{E}_{\Omega_1}$ in (9b) and substituting it back into (9a), we obtain:

$$\begin{aligned}\mathbf{A}_{\partial\Omega_1}(s)\mathbf{E}_{\partial\Omega_1} + \mathbf{F}_{\Omega_0\delta}^T(s)\mathbf{E}_{\Omega_0}&\\ - \mathbf{F}_{\Omega_1\delta}^T(s)\mathbf{A}_{\Omega_1}^{-1}(s)\mathbf{F}_{\Omega_1\delta}(s)\mathbf{E}_{\partial\Omega_1} &= 0.\end{aligned} \tag{10}$$

Here, we can define a transfer function that describes the input-output behavior in subdomain Ω_1, viz.

$$\begin{aligned}\mathbf{H}_{\Omega_1}(s) &= -\mathbf{F}^T_{\Omega_1\delta}(s)\mathbf{A}^{-1}_{\Omega_1}(s)\mathbf{F}_{\Omega_1\delta}(s) \\ &= -\left(\mathbf{G}^T_{\Omega_1\delta} + s^2\mathbf{T}^T_{\Omega_1\delta}\right)\cdot \\ &\cdot\left(\mathbf{\Gamma}_{\Omega_1} + s^2\mathbf{C}_{\Omega_1}\right)^{-1}\left(\mathbf{G}_{\Omega_1\delta} + s^2\mathbf{T}_{\Omega_1\delta}\right).\end{aligned} \tag{11}$$

Note that the poles of this transfer function are the same as the eigenvalues of the matrix pencil $(\mathbf{\Gamma}_{\Omega_1}, \mathbf{C}_{\Omega_1})$ and, as observed above, they are also the poles of the admittance matrix for this subdomain as well as the resonances of a PEC cavity formed by this subdomain.

Next, local order reduction is performed for region Ω_1. The projection space $\mathbf{Q}$ is found using the technique described in [34]. As explained there, in order to account for nonaffine parameter dependence, the basis is formed by concatenating and then processing the orthogonal bases obtained for M different parameter samples, which may include geometry changes:

$$\mathbf{Q} = [\mathbf{Q}_1\ \mathbf{Q}_2 \ldots \mathbf{Q}_M]. \tag{12}$$

Each basis is calculated as described in [13]. The subsequent processing, which involves a two stage compression process using singular value decomposition (SVD) and proper orthogonal decomposition (POD), makes the basis more compact.

Applying the Galerkin projection to the specific system of equations gives rise to the reduced matrices that replace the large sparse FEM matrices in the original system of equations:

$$\begin{aligned}\widetilde{\mathbf{\Gamma}}_{\Omega_1} &= \mathbf{Q}^T\mathbf{\Gamma}_{\Omega_1}\mathbf{Q}, \quad \widetilde{\mathbf{C}}_{\Omega_1} = \mathbf{Q}^T\mathbf{C}_{\Omega_1}\mathbf{Q}, \\ \widetilde{\mathbf{G}}_{\Omega_1\delta} &= \mathbf{Q}^T\mathbf{G}_{\Omega_1\delta}, \quad \widetilde{\mathbf{T}}_{\Omega_1\delta} = \mathbf{Q}^T\mathbf{T}_{\Omega_1\delta}.\end{aligned} \tag{13}$$

The size of the resultant matrices is much smaller than the originals. The reduced matrices are substituted back to the original FEM problem, replacing the appropriate rows and columns of the full-order system and thus reducing its size. The reduced form of the transfer function $\widetilde{\mathbf{H}}_{\Omega_1}(s)$, which approximates the original transfer function over a wide frequency band, is defined as follows:

$$\begin{aligned}\widetilde{\mathbf{H}}_{\Omega_1}(s) = -\left(\widetilde{\mathbf{G}}^T_{\Omega_1\delta} + s^2\widetilde{\mathbf{T}}^T_{\Omega_1\delta}\right)\left(\widetilde{\mathbf{\Gamma}}_{\Omega_1} + s^2\widetilde{\mathbf{C}}_{\Omega_1}\right)^{-1}\cdot \\ \cdot\left(\widetilde{\mathbf{G}}_{\Omega_1\delta} + s^2\widetilde{\mathbf{T}}_{\Omega_1\delta}\right).\end{aligned} \tag{14}$$

It should be noted that the matrix that is inverted becomes singular at the frequencies that are the eigenvalues of the matrix pencil $(\widetilde{\mathbf{\Gamma}}_{\Omega_1}, \widetilde{\mathbf{C}}_{\Omega_1})$, which are also approximate eigenresonances of the PEC cavity formed by subdomain Ω_1.

III. Nonphysical Poles

As an illustration of the problem discussed in this paper, we consider a parametrized model of a fifth-order waveguide filter [37]. The structure is divided into seven subdomains. Its geometry and segmentation analysis are shown in Fig. 1. For this structure, a total of eleven geometry parameters are considered, some of them in different regions of the analysis domain. As such, there are 2, 2, 3, 2, and 2 design

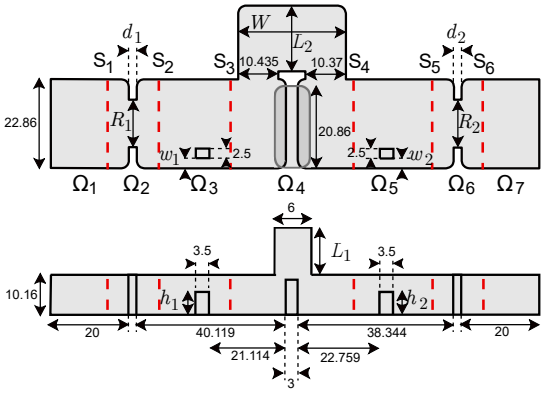

Fig. 1. Geometry of a fifth-order waveguide filter divided into seven subdomains.

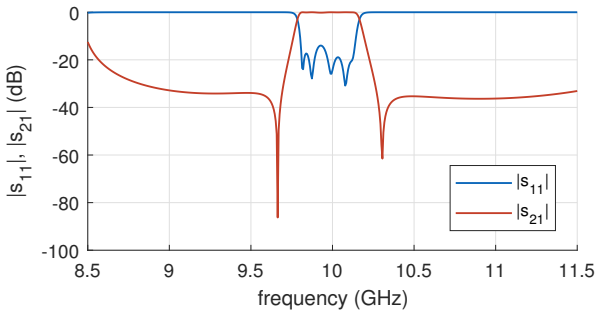

Fig. 2. Reference scattering parameters in the fifth-order waveguide filter computed using the full-order FEM model.

variables in corresponding regions Ω_2, Ω_3, Ω_4, Ω_5 and Ω_6, respectively. For reference, we first ran the simulations for a full-order FEM model for all eleven design parameters set to the values given in the third column of Table I. The reference scattering characteristics of the filter for the frequency band 8.5-11.5 GHz are shown in Fig. 2.

For this structure, we will take into account PROMs for each of the five subdomains where the design variables change, each one using multiple concatenated local bases, created for several parameter samples taken within the allowable range of geometry variation defined by the fourth and fifth columns in Table I. The geometry instances used to generate the local PROMs are different from the ones that we use as reference points. Our goal is to use the local PROMs to reproduce the reference characteristics computed from the full-order FEM model, i.e. the original FEM equations, for the entire structure.

We initially consider only one local PROM associated with region Ω_5. In constructing this PROM for region Ω_5, we used four local bases generated for the geometry instances detailed in Table II. We deliberately selected rather large offsets from the reference point to ensure a low-quality local PROM, making the problem we want to address more conspicuous.

The scattering characteristics of this filter computed with the basis we have described earlier for region Ω_5 are shown in Fig. 3. Some artifacts, in the form of spikes, are clearly visible. These artifacts evidently have a resonant character. To confirm this, we computed a few eigenvalues of the full-

TABLE I
REFERENCE VALUES OF GEOMETRY PARAMETERS AND VARIATION RANGE FOR GEOMETRY SAMPLES USED TO CREATE LOCAL BASES

domain	parameter	reference (mm)	min (mm)	max (mm)
Ω_2	d_1	2.000	1.000	3.000
	R_1	12.188	10.188	14.188
Ω_3	h_1	5.456	2.450	8.450
	w_1	2.430	1.430	5.430
Ω_4	W	27.805	26.805	28.805
	L_1	12.194	8.194	16.194
	L_2	16.743	12.743	20.743
Ω_5	h_2	5.949	2.949	8.949
	w_2	2.430	1.430	5.430
Ω_6	d_2	2.000	1.000	3.000
	R_2	12.264	10.264	14.264

TABLE II
CHANGE IN GEOMETRY PARAMETERS FROM REFERENCE VALUES IN Ω_5 FOR GEOMETRY INSTANCES $\mathcal{G}_1, \mathcal{G}_2, \mathcal{G}_3, \mathcal{G}_4$ USED TO GENERATE A COMBINED LOCAL PROJECTION BASIS

parameter offset	$\mathcal{G}_1$	$\mathcal{G}_2$	$\mathcal{G}_3$	$\mathcal{G}_4$
h_2 [mm]	-2.3	-2.39	-1.64	-2.23
w_2 [mm]	-1.39	1.28	2.45	-1.1

order FEM model and the model using a local PROM. These eigenvalues correspond to the poles of the admittance matrix of the complete structure and define the resonances of the cavity formed by short-circuiting the ports, i.e., replacing the ports with PEC. The results are presented in Table III. The full-order FEM model, detailed in the left column, shows five resonances, as can be expected from a fifth-order bandpass filter. A model involving a local PROM, detailed in the right column, exhibits twelve nonphysical resonances in addition the true resonances, which are shown in bold.

Evidently, the artifacts render this particular local PROM inadmissible for practical use. This does not mean that the technique of local PROMS employing concatenated bases is of little value. As indicated above, we have selected a particularly bad local PROM for illustration purposes. In fact, the poor quality of this model would have been detected using a local error estimator [35]. If the level of the local error estimator were too high, the local basis would have been augmented as

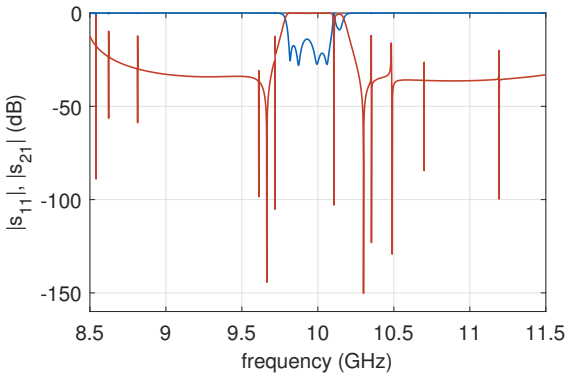

Fig. 3. Scattering parameters of the fifth-order waveguide filter with several artifacts due to local PROM in region Ω_5 generated by concatenation of four projection bases evaluated at the points given in Table II.

TABLE III
RESONANCES OF THE FULL-ORDER MODEL AND A FORMULATION WITH ONE LOCAL PROM

Frequency (GHz)	Frequency (GHz)		
9.7658	8.5408	**9.7659**	**10.1643**
9.8120	8.6231	**9.8120**	10.3515
9.9450	8.8139	**9.9449**	10.4829
10.0758	9.3407	**10.0690**	10.6994
10.1578	9.6113	10.1102	11.1501
	9.7185		11.1917

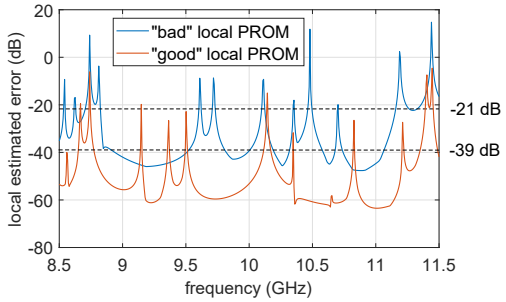

Fig. 4. Local error estimator for good and bad nonregularized PROMs for region Ω_5 in the fifth-order waveguide filter.

recommended in [34]. Fig. 4 shows the plots of the local error estimators for this bad local PROM, detailed in blue, and for a good local PROM, plotted in orange. It can be seen that the average value for the error estimator for the good model is almost -40 dB, while for the model created with the bases evaluated for geometries given in Table II, this value is much higher.

While this model is evidently poor, it should be noted that, except for the few spikes visible in Fig. 3, the overall characteristics do not look especially bad. The true poles of the system are also quite well reproduced, as it is clear from Table III. For this reason, it is worth looking for simple and cost efficient ways of predicting and preventing these artifacts from appearing without resorting to the addition of new vectors to the local basis, as this would eventually make local PROMs too large.

IV. IDENTIFYING AND ELIMINATING NONPHYSICAL POLES

A better insight into the nature of the artifacts observed when local PROMs are used in simulations can be gained by examining the poles of the transfer function (14) for a local PROM as new local projection bases are added and concatenated to form a single projection basis. The poles of the local transfer function for the reduced model are the eigenvalues of the system matrices obtained after projection. Fig. 5 shows the eigenvalue spectrum for the matrix pencil $(\widetilde{\mathbf{\Gamma}}_{\Omega_5}, \widetilde{\mathbf{C}}_{\Omega_5})$ in region Ω_5 in the fifth-order waveguide filter for different projection bases. Only the eigenvalues located in the filter bandwidth are shown.

The eigenvalues are denoted by crosses or circles and are presented on five lines, corresponding to five bases. The first line in the bottom shows the reference eigenvalues, i.e., the eigenvalues found for the correct basis $\mathbf{Q}^{\mathcal{P}} = \mathbf{Q}_0$. This

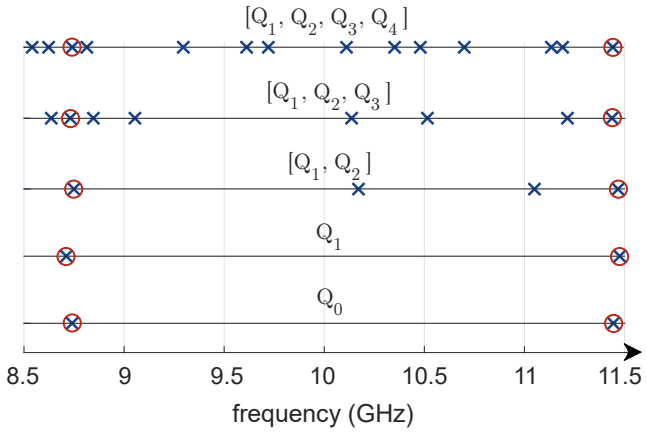

Fig. 5. Eigenvalues of the local PROM in region Ω_5 in the fifth-order waveguide filter obtained using different local projection bases.

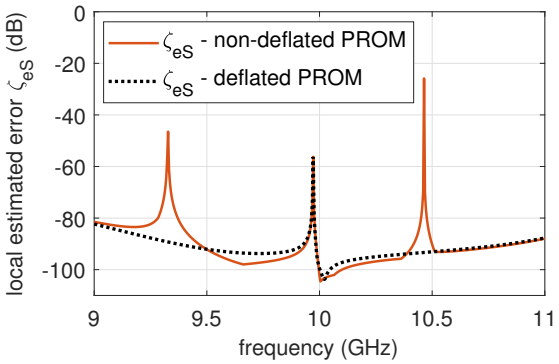

Fig. 6. Local estimated error [35] in subdomain Ω_4 after removing two nonphysical poles from the PROM in the waveguide filter, compared to the estimated local error before deflation.

basis is evaluated for the references values of parameters, $h_2 = 5.949$ mm, $w_2 = 2.430$ mm. The second bottom line is for the basis obtained for the geometry instance $\mathcal{G}_1$ in Table II. In other words, here we use $\mathbf{Q}^{\mathcal{P}} = \mathbf{Q}_1$. The next line in Fig. 5 uses the basis obtained by concatenation of $\mathbf{Q}_1$ and $\mathbf{Q}_2$, that is, the bases evaluated for the instances $\mathcal{G}_1$ and $\mathcal{G}_2$ in Table II. Finally, the line on the top is for $\mathbf{Q}^{\mathcal{P}} = \text{SVD}([\mathbf{Q}_1,\ \mathbf{Q}_2,\ \mathbf{Q}_3,\ \mathbf{Q}_4])$.

From this example shown in Fig. 5, it is clear that as soon as the number of geometry instances, in other words, concatenated bases, exceeds one, new eigenvalues begin to appear in addition to the correct ones, which are denoted by circles in Fig. 5. These additional eigenvalues are nongenuine poles of a local transfer function—nonphysical resonances of a PEC cavity corresponding to a given subdomain. This phenomenon is understandable if we consider the fact that each basis spans a *similar* space, in the sense that the maximum eigenvalue for each local PROM obtained with each of the local projection basis is expected to be similar. No local basis can approximate the eigenvectors that are outside this range. If the size of each basis is, say, K, each local PROM will have exactly K poles distributed between 0 and a certain $f_{\max}$. Consequently, when we concatenate i bases, a local PROM will have $i \cdot K$ poles, and these poles will be distributed across a comparable frequency band. In this scenario, we can expect that there will be exactly $(i-1) \cdot K$ bogus, or *ghost*, poles. In practice, when the procedure proposed in [34] is used, the number of nonphysical resonances will be smaller, as once several bases are concatenated, the resulting basis is compressed twice. Nevertheless, if many geometry instances are used, the number of nonphysical poles may be substantial, although not all of them will produce conspicuous artifacts in the frequency characteristics, i.e., the quality of the combined basis confirmed by the local error estimate may be satisfactory, or the *ghost* pole may be outside the band of interest.

Obviously, the simplest way to get rid of the artifacts would be to eliminate all poles that fall in a given band. This strategy would however fail if the size of the subdomain were large enough to allow for physical resonances. Rather than reducing the size of the subdomain, we need a technique to identify *ghost* poles in the band of interest and to distinguish them from true resonances. In the next section, we present two such techniques for regularizing local PROMs.

A. Regularization Based on Ritz Pairs

One way to check if the eigenvalue in a local PROM is a nongenuine pole or a correct resonance is to verify how well this eigenvalue and the associated eigenvector, or strictly speaking, the Ritz value and Ritz vector, satisfy the eigenvalue equation when they are substituted into the local full-order FEM model. To this end, the residues for a full-order model are computed for all Ritz values and Ritz vectors that are to be examined. A Ritz pair that corresponds to large values of the norm of the residual relates to a false pole, while a small value of the norm is obtained for legitimate resonances.

When the set of Ritz values and vectors corresponding to nonphysical poles is identified, the Gram–Schmidt orthogonalization procedure can be used to find the new basis $\widetilde{\mathbf{Q}}^{\mathcal{P}}$, which is $\mathbf{C}_{\Omega_j}$-orthogonal to these vectors. To this end, each vector of $\mathbf{Q}^{\mathcal{P}}$ is $\mathbf{C}$-orthogonalized to every Ritz vector and, in effect, the deflated subspace spanned by the basis $\widetilde{\mathbf{Q}}^{\mathcal{P}}$ is obtained.

To illustrate this process, we consider a local PROM for subdomain Ω_4 in the fifth-order waveguide filter detailed in Fig. 1. We used three geometry instances to generate a local projection basis. This resulted in a PROM with three poles in the band of interest: at 9.3271, 9.9716, and 10.4640 GHz. The Ritz vectors were computed for these poles, yielding the following values for the residual errors: 0.0918, $2.49 \cdot 10^{-5}$, and 0.1089, respectively. One pole, located at 9.9716 GHz, brings about a much smaller residual error than the other two. We can infer that this is a true resonance, while the other two are nonphysical and should be removed. The deflation is performed by making the projection basis $\mathbf{C}_{\Omega_4}$-orthogonal to two Ritz vectors identified as the nongenuine ones. Fig. 6 shows a local estimated error in subdomain Ω_4 before and after the removal of two nonphysical poles from the PROM. The two false poles no longer exist in the reduced-order model.

While the regularization strategy based on Ritz pairs works, it may prove inefficient, particularly for large projection basis. Note that it is necessary to compute the residues of the

TABLE IV
POLES (IN GHZ) OF THE WAVEGUIDE FILTER MODEL INVOLVING FIVE LOCAL PROMS

9.7660	9.7664	9.5076	9.3271	9.0405
9.8123		10.002	10.4640	9.1134
9.9453		10.6363		9.3488
10.0760		10.7804		9.6035
10.1579				10.0845
				10.6862
				10.8953

TABLE V
POLES (IN GHZ) OF THE WAVEGUIDE FILTER OF FIVE LOCAL PROMS: $\Omega_2, \Omega_3, \Omega_4, \Omega_5, \Omega_6$

Ω_2	Ω_3	Ω_4	Ω_5	Ω_6
9.7663	9.5076	9.3271	9.0405	-
	10.0020	**9.9716**	9.1134	
	10.6363	10.4640	9.3488	
	10.7804		9.6037	
			10.0844	
			10.6862	
			10.8952	

Ritz vectors for the full-order FEM model, then to perform the Gram–Schmidt procedure, and finally to construct the new reduced-order model by orthogonal projection onto the deflated subspace. These operations involve nonreduced matrices, so when there are many vectors in the basis, the total time may be noticeable. The time needed for these operations in the above example on a workstation detailed in Sec. V is 6.4 s. Computation of the residues of three Ritz vectors took 1.0 s, constructing the new basis with the Gram–Schmidt procedure took 1.95 s, and orthogonal projection took 3.4 s. When this strategy is applied to multiple PROMs, the overall time may be significant.

B. Regularization Based on the Bauer–Fike Theorem

To this end, we evaluated the poles of the admittance matrix located in the frequency band 9–11 GHz for the reduced-order model of the whole waveguide filter involving five local PROMs. The results are listed in Table IV. Bold text denotes the poles that are also present in the full-order FEM model given in the first column of Table III. Eigenvalue analysis was then carried out for all five local PROMs when each of these is considered separately from the others. Table V shows the poles within the same band for each of the five examined subdomains Ω_2, Ω_3, Ω_4, Ω_5 and Ω_6. Note that all nonphysical poles from Table IV can be identified in Table V as eigenvalues related to individual local PROMs for certain subdomains. It is clear that these eigenvalues are nonphysical resonances and should be deflated so as not to pollute the solution obtained for the complete structure. Note also that one eigenvalue for subdomain Ω_4, shown in bold in Table V, cannot be identified in Table IV. However, as was shown in the previous section by evaluating the residual associated with the Ritz pairs, this eigenvalue corresponds to an actual resonance. Note also that the other two eigenvalues for subdomain Ω_4 have already been shown to be nonphysical resonances.

We see that false poles in local PROMs can be identified by verifying whether they have counterparts in the global PROM. All eigenvalues that are present in both the local model and the global system involving all PROMs are nongenuine poles. However, we do not recommend this approach, a simpler procedure for deflating false poles is needed. Instead of comparing two sets of eigenvalues, we will thus use the fact that the physical and nonphysical resonances in local PROMs behave differently when they are incorporated into the system of equations for the entire structure. From the tables above, we can see that while nonphysical poles do not move when local PROMs are assembled, i.e., they are at almost the same place in the local and global models, the true local resonances in subdomain Ω_4 can no longer be identified in the global model. This means that nonphysical local resonances are localized and are not affected by neighboring subdomains, while the true resonances interact with the surrounding regions.

This observation suggests that a technique for regularizing local PROMs, i.e., identifying and deflating nonphysical poles, can be developed by concentrating on the impact of the surrounding regions. The eigenvalues not affected by incorporating a local PROM into the global system will be regarded as false poles and deflated by removing the eigenvector that is associated with this eigenvalue. To this end, we use the Bauer–Fike theorem [38] for generalized eigenvalue problems and compute the bounds of the shift the eigenvalues undergo when matrices related to local PROMs are influenced by the presence of other subregions. Let $(\lambda_{0_i}, \mathbf{x}_{0_i})$ be an eigenvalue and the corresponding eigenvector of a Hermitian matrix pencil $(\mathbf{A}_0, \mathbf{B}_0)$ with positive definite $\mathbf{B_0}$, so that

$$(\mathbf{A}_0 - \lambda_{0_i}\mathbf{B}_0)\mathbf{x}_{0_i} = 0. \tag{15}$$

The Bauer–Fike theorem provides the error bound for the eigenvalue when both matrices are perturbed. Assuming that λ_i denotes an eigenvalue of the perturbed pencil $(\mathbf{A}_0 + \mathbf{\Delta A}, \mathbf{B}_0 + \mathbf{\Delta B})$, the error bound $\Delta\lambda_{i(est)}$ for i-th eigenvalue is given by

$$|\widetilde{\lambda_i} - \lambda_i| \leq \Delta\lambda_{i(est)} = \| \, (\mathbf{B}_0 + \mathbf{\Delta B})^{-1} \, \| \cdot \| \, \mathbf{r} \, \|, \tag{16}$$

where $\| \, \mathbf{r} \, \|$ is a norm of the residual vector

$$\| \, \mathbf{r} \, \| = \| \, (\mathbf{\Delta A} - \lambda_{0_i}\mathbf{\Delta B})\mathbf{x}_{0_i} \, \| \, . \tag{17}$$

In order to show how to use the Bauer–Fike theorem for our purpose, we consider the situation where all local PROMs have been substituted into FEM matrices. The resulting system of equations consists of small and dense blocks, namely, macromodels, and for the fifth-order waveguide filter in Fig. 1 this system has the sparsity pattern shown in Fig. 7. Consider subdomain Ω_4. The behavior of the electromagnetic field in subdomain Ω_4 is determined by the following local projected system of equations:

$$(\widetilde{\mathbf{\Gamma}}_{\Omega_4} + s^2\widetilde{\mathbf{C}}_{\Omega_4})\widetilde{\mathbf{E}}_{\Omega_4} = -(\widetilde{\mathbf{G}}_{\Omega_4\delta} + s^2\widetilde{\mathbf{T}}_{\Omega_4\delta})\mathbf{E}_{\partial\Omega_4} \tag{18}$$

where $\widetilde{\mathbf{G}}_{\Omega_4\delta}$ and $\widetilde{\mathbf{T}}_{\Omega_4\delta}$ are the reduced blocks describing the coupling between subregion Ω_4 and interfaces S_3, S_4 in Fig. 1. $\widetilde{\mathbf{E}}_{\Omega_4}$ contains coefficients associated with the electric field in the interior of subdomain Ω_4 and $\widetilde{\mathbf{E}}_{\partial\Omega_4}$ contains coefficients associated with the electric field on the boundary $\partial\Omega_4$.

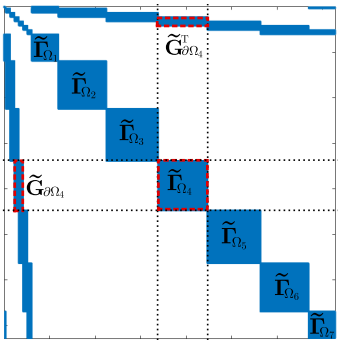

Fig. 7. Sparsity pattern of the reduced matrix $\widetilde{\mathbf{\Gamma}}$ in the fifth-order waveguide filter in Fig. 1.

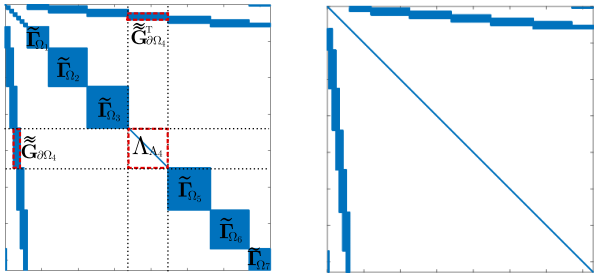

Fig. 8. (a) Sparsity pattern of the reduced matrix stiffness $\widetilde{\mathbf{\Gamma}}$ with one diagonalized macromodel Ω_4. (b) Sparsity pattern of completely diagonalized reduced stiffness matrix $\widetilde{\mathbf{\Gamma}}$ with five local PROMs).

This local system has the form:

$$(\widetilde{\mathbf{\Gamma}}_{\Omega_4} + s^2\widetilde{\mathbf{C}}_{\Omega_4})\widetilde{\mathbf{E}}_{\Omega_4} = -\widetilde{\mathbf{F}}_{\Omega_4\delta}(s)\mathbf{E}_{\partial\Omega_4} \tag{19}$$

with both matrices $\widetilde{\mathbf{\Gamma}}_{\Omega_4}, \widetilde{\mathbf{C}}_{\Omega_4}$ being symmetric and $\widetilde{\mathbf{C}}_{\Omega_4}$ positive definite. $\widetilde{\mathbf{F}}_{\Omega_4\delta}$ represents the coupling matrices on the right-hand side of equation (18)

$$\widetilde{\mathbf{F}}_{\Omega_4\delta}(s) = \widetilde{\mathbf{G}}_{\Omega_4\delta} + s^2\widetilde{\mathbf{T}}_{\Omega_4\delta}. \tag{20}$$

Using the technique described in the Appendix, we can now diagonalize both matrices in the local system. Performing the necessary steps, we first obtain

$$(\mathbf{A}_4 + s^2\mathbf{Id})\widetilde{\mathbf{C}}_{\Omega_4}^{\frac{1}{2}}\widetilde{\mathbf{E}}_{\Omega_4} = -\widetilde{\mathbf{C}}_{\Omega_4}^{\frac{1}{2}}\widetilde{\mathbf{F}}_{\Omega_4\delta}(s)\mathbf{E}_{\partial\Omega_4}, \tag{21}$$

where $\mathbf{Id}$ is the identity matrix and $\mathbf{A}_4$ is a symmetric matrix

$$\mathbf{A}_4 = \widetilde{\mathbf{C}}_{\Omega_4}^{-\frac{1}{2}}\widetilde{\mathbf{\Gamma}}_{\Omega_4}\widetilde{\mathbf{C}}_{\Omega_4}^{-\frac{1}{2}}. \tag{22}$$

Next, we perform the eigendecomposition of the symmetric matrix $\mathbf{A}_4$:

$$\mathbf{A}_4 = \mathbf{V}_{A_4}\mathbf{\Lambda}_{A_4}\mathbf{V}_{A_4}^T \tag{23}$$

and convert equation (21) into:

$$(\mathbf{\Lambda}_{A_4} + s^2\mathbf{Id})\underbrace{\mathbf{V}_{A_4}^T\widetilde{\mathbf{C}}_{\Omega_4}^{\frac{1}{2}}\widetilde{\mathbf{E}}_{\Omega_4}}_{\hat{\mathbf{E}}_{\Omega_4}} = -\mathbf{V}_{A_4}^T\widetilde{\mathbf{C}}_{\Omega_4}^{\frac{1}{2}}\widetilde{\mathbf{F}}_{\Omega_4\delta}(s)\mathbf{E}_{\partial\Omega_4}. \tag{24}$$

The left-hand side of this equation is a diagonal matrix and the matrix $\mathbf{\Lambda}_{A_4}$ contains the poles of the local PROM. Once the required operations are completed, the entire system has the structure shown in Fig. 8a.

Diagonalization of the left-hand side involves computing the square root of matrix $\mathbf{C}$ and its inverse, and then eigendecomposing matrix $\mathbf{A} = \mathbf{C}^{-1/2}\mathbf{\Gamma}\mathbf{C}^{-1/2}$. See Appendix for all the details. Since the projected matrices are small, computing the square root of $\mathbf{C}$ as in (27), computing its inverse (29), and performing the eigendecomposition of matrix $\mathbf{A}$ is fast. It is, however, an effort that pays off, as now the poles of PROM for subdomain Ω_4 are on the diagonal and the couplings are expressed only by the off-diagonal elements. Since the matrix is symmetric, it is enough to consider the values of the off-diagonal elements that are in the same row as the pole we are interested in. The time needed for the diagonalization of this local PROM was just 0.1444 s.

The diagonalization can be repeated for all diagonal blocks, and ultimately, the matrix receives the bordered diagonal form shown in Fig. 8b.

1) Deflation: Once the complete diagonalization of all diagonal blocks has been performed, we may split the reduced-order system matrix for the entire structure into the diagonal part and the part with all off-diagonal elements, and then apply the Bauer–Fike theorem to the diagonal part, taking the off-diagonal elements as the perturbation. Referring to equation (15) $\mathbf{A}_0 = \mathbf{\Lambda}_A$, i.e., a diagonal matrix with all poles, and $\mathbf{B}_0 = \mathbf{Id}$, while $\mathbf{\Delta A}$ and $\mathbf{\Delta B}$, are block matrices with zeroes on the diagonal and nonzero elements located in the first group of rows and columns. The set of eigenvalues of the pencil $(\mathbf{A}_0, \mathbf{B}_0)$ consists of all poles, and the eigenvector associated with the i-th diagonal element is a vector with all zeros, except for the i-th element, which is equal to one. The perturbation for a given pole is related only to the value of the residual. Its computation is trivial as it requires only the evaluation of the norm of a rather short vector consisting of nonzero off-diagonal elements in the i-th row of the perturbation, namely coupling matrices. If this residual is small, the eigenvalue is not sensitive to the coupling and so it must be a ghost pole. Deleting this pole is now trivial: it suffices to zero out the row and column corresponding to this pole.

V. Validation of the Regularization Procedure

To validate the proposed identification and deflation procedure, we have performed a number of tests. All computations were carried out on a workstation with an AMD Ryzen 7 (3.39 GHz) processor and 64 GB RAM.

A. Test 1: Fifth-order filter with eleven variables and five local PROMs

In this test, we consider a fully parametrized model of the filter shown in Fig. 1, where the segmentation scheme is also depicted. In constructing the local PROMs, we used the following number of geometry instances corresponding to the number of local bases in the subdomains: 2 for subdomain Ω_2, 3 for Ω_3, 3 for Ω_4, 3 for Ω_5, and 2 for Ω_6. The frequency response of the filter in the 9-11 GHz band, obtained from

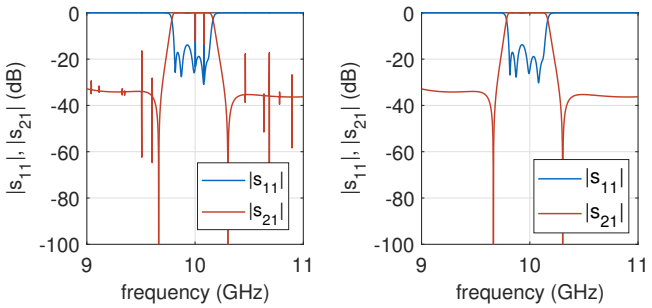

Fig. 9. Waveguide filter response prior to regularization (a) and after regularization (b).

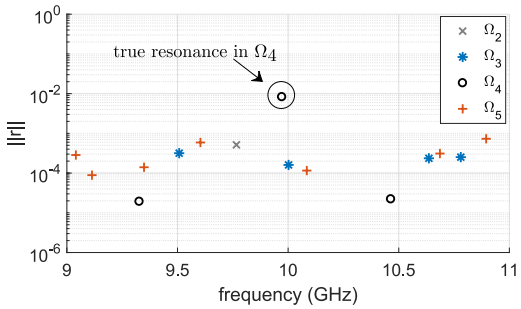

Fig. 10. Perturbation bounds for all local eigenvalues in the PROMs in the band of analysis obtained by the Bauer–Fike theorem.

the reduced-order system prior to regularization, is shown in Fig. 9a.

There were fifteen poles in the frequency band of interest. Fig. 10 shows the value of the perturbation bounds for all local eigenvalues in the PROMs obtained by the Bauer–Fike theorem. It is evident that all but one of the poles are nonphysical. All the local PROMs were regularized by zeroing out appropriate rows and columns in the reduced-order system. The frequency characteristics for the filter after deflation are shown in Fig. 9b.

The error bound may also be easily computed for out-of-band eigenvalues. Based on this, 25 eigenvalues of the PROM of subdomain Ω_2 were identified as false and deflated. Similarly, 46, 16, 48, and 28 eigenvalues were removed from the PROMs in subdomains Ω_3, Ω_4, Ω_5, Ω_6, respectively. This reduced the size of the reduced-order model for the entire structure from 1456 to 1293. The time needed to obtain the diagonal form of the reduced FE matrices was 0.42 s, while computing the perturbation bounds for all the local eigenvalues of the five PROMs took only 0.16 s. The overall time needed to regularize all five PROMs, involving the elimination of 163 nonphysical poles, was just 0.58 s. This is much faster than regularization based on Ritz pairs, where the deflation of only two nonphysical poles in just one PROM for subdomain Ω_4 took 6.4 s.

We have also calculated the poles inside the band of interest for the entire structure after deflating the nonphysical poles in macromodels. This resulted in five values: 9.7660, 9.8123, 9.9453, 10.0761, 10.1579 GHz, that are consistent with the

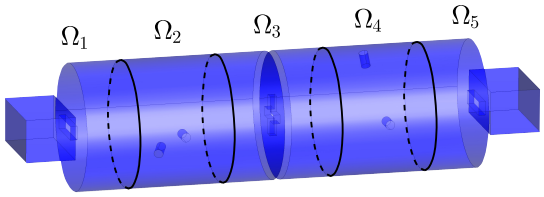

Fig. 11. Dual-mode filter segmented into five subdomains. The dimension of the structure can be found in [1].

poles determined for the full-order system given in the first column in Table III.

B. Test 2: Dual-mode filter with six design variables and three local PROMs

In the second test, we considered the dual-mode waveguide filter shown in Fig. 11. The frequency band of interest was 11.4–13.4 GHz and was extended well beyond the passband of the filter. The structure was segmented into five subdomains: Ω_1, Ω_2, Ω_3, Ω_4, and Ω_5, as detailed in Fig. 11. Local multivariate reduced-order models were created for subdomains Ω_2, Ω_3 and Ω_4, where the lengths of four tuning screws and the lengths of the two arms of the cross-shaped iris were regarded as parameters. In order to construct the PROMs, three local bases associated with three different geometries were used in both Ω_2 and Ω_4, while two bases were used in Ω_3. This resulted in nonphysical poles of the PROM, which can be seen in the frequency response shown in Fig. 12a. As a matter of fact, there are many spikes but, interestingly enough, some of them are legitimate, and occur also when the filter is analyzed frequency-by-frequency using standard FEM, while other are bogus. True spikes are due to higher order modes of filter cavities, while the rest is due to PROMs. Without a good regularization procedure it would be impossible to distinguish one category of spikes from the others and to remove nongenuine poles.

Computing the resonant frequencies of the reduced-order model involving three local PROMs resulted in 57 values in the band 11.4–13.4 GHz, of which only 17 are true resonances.

Next, the local reduced matrices were diagonalized one by one and the residues defined in (17) were computed. Fig. 13 shows the residues computed for all eigenvalues in the band of analysis. From Fig. 13, it is apparent that there are multiple nonphysical resonances with residues below 10^{-2}, which should be deflated.

However, it is also worth observing the residues of all the poles, including the out-of-band ones. Fig. 14 shows the residues of all eigenvalues of the local PROM up to 40 GHz. Based on the Bauer–Fike theorem, 42, 47 and 50 resonances have been identified as nongenuine in subdomains Ω_2, Ω_3 and Ω_4, respectively, i.e., the resonances with residues below 10^{-2} in Fig. 14. The scattering parameters computed for the deflated reduced-order model are presented in Fig. 12b. Good agreement with the reference filter response is obtained. In order to further validate the quality of the regularized PROM, the resonances of the global model after deflation were computed, and this resulted in 17 resonant frequencies in the band of analysis, corresponding to the poles of the admittance

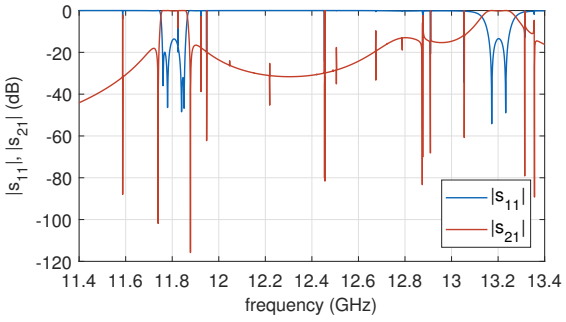

(a)

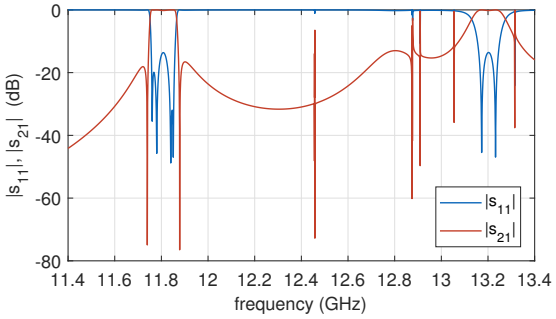

(b)

Fig. 12. (a) Scattering parameters computed with the FEM-PMOR technique: The effect of nonphysical resonances in the band. (b) Scattering parameters obtained for deflated ROM—good agreement with the results obtained with direct FEM analysis.

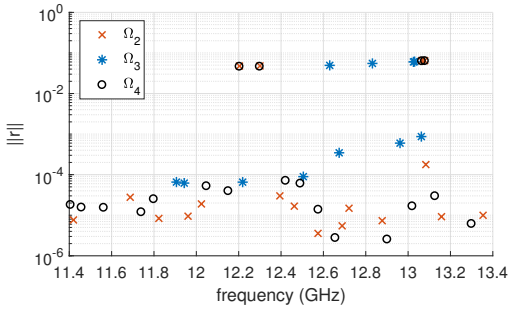

Fig. 13. Perturbation bounds for eigenvalues of the PROMs in frequency band of analysis.

matrix of the model with no local PROMs, and where there were no nonphysical resonances.

VI. Conclusions

A problem relating to artifacts that occur in parametrized model order reduction using subspace projection has been discussed. It has been shown that these artifacts, which take the form of spikes in the frequency characteristics, are a result of nonphysical poles of the transfer function that emerge if a parametrized model is created by projecting the original system of equations onto a subspace spanned by a set of vectors, when this subspace is formed by combining into a single basis several bases created by sampling a parameter space. A simple technique using the Bauer–Fike theorem was

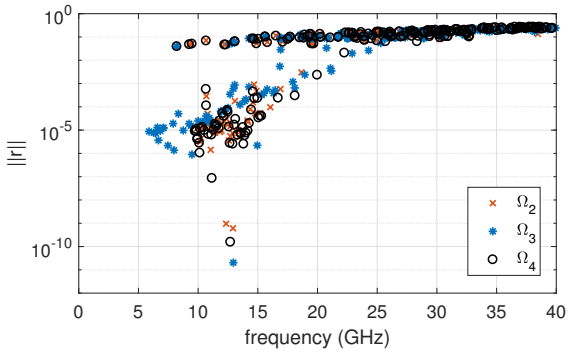

Fig. 14. Perturbation bounds for all eigenvalues of the PROMs up to 40 GHz - 139 eigenvalues below 10^{-2} have been deflated from the local PROMs.

proposed to remove unwanted poles and its efficiency was validated on problems involving bandpass filters.

Appendix
The Diagonalization of Matrices

We consider a set of linear equations in the form

$$(\mathbf{\Gamma} + s^2\mathbf{C})\mathbf{x} = \mathbf{b} \tag{25}$$

with both matrices $\mathbf{\Gamma}, \mathbf{C}$ being symmetric and $\mathbf{C}$ positive definite. We define $\tilde{\mathbf{x}} = \mathbf{C}^{1/2}\mathbf{x}$. To find the square root of the matrix $\mathbf{C}$, we compute its eigendecomposition

$$\mathbf{C} = \mathbf{W}\mathbf{\Sigma}\mathbf{W}^T, \tag{26}$$

where $\mathbf{\Sigma}$ is a diagonal matrix of eigenvalues of $\mathbf{C}$ and $\mathbf{W}$ is an orthogonal matrix containing eigenvectors of $\mathbf{C}$. Then

$$\mathbf{C}^{1/2} = \mathbf{W}\mathbf{\Sigma}^{1/2}\mathbf{W}^T, \tag{27}$$

where $\mathbf{\Sigma}^{1/2}$ is a diagonal matrix with the square roots of the eigenvalues of $\mathbf{C}$ on its diagonal.

We now rewrite (25) as

$$\left(\mathbf{\Gamma}\mathbf{C}^{-1/2}\mathbf{C}^{1/2} + s^2\mathbf{C}^{1/2}\mathbf{C}^{1/2}\right)\mathbf{x} = \mathbf{b}, \tag{28}$$

where

$$\mathbf{C}^{-1/2} = \mathbf{W}\mathbf{\Sigma}^{-1/2}\mathbf{W}^T. \tag{29}$$

Since $\tilde{\mathbf{x}} = \mathbf{C}^{1/2}\mathbf{x}$, the multiplication by $\mathbf{C}^{-1/2}$ gives rise to

$$\left(\mathbf{C}^{-1/2}\mathbf{\Gamma}\mathbf{C}^{-1/2} + s^2\mathbf{Id}\right)\tilde{\mathbf{x}} = \mathbf{C}^{-1/2}\mathbf{b}. \tag{30}$$

We now denote $\mathbf{A} = \mathbf{C}^{-1/2}\mathbf{\Gamma}\mathbf{C}^{-1/2}$ and perform a spectral decomposition of the matrix $\mathbf{A}$:

$$\mathbf{A} = \mathbf{V}_A\mathbf{\Lambda}\mathbf{V}_A^T, \tag{31}$$

where $\mathbf{\Lambda}$ is a diagonal matrix of eigenvalues of $\mathbf{A}$ and $\mathbf{V}$ is an orthogonal matrix containing eigenvectors. With this result, we obtain

$$\mathbf{V}_A\left(\mathbf{\Lambda} + s^2\mathbf{Id}\right)\mathbf{V}_A^T\tilde{\mathbf{x}} = \mathbf{C}^{-1/2}\mathbf{b}. \tag{32}$$

Finally, left multiplication by $\mathbf{V}_A^T$ gives

$$\left(\mathbf{\Lambda} + s^2\mathbf{Id}\right)\mathbf{V}_A^T\mathbf{C}^{1/2}\mathbf{x} = \mathbf{V}_A^T\mathbf{C}^{-1/2}\mathbf{b}. \tag{33}$$

REFERENCES

[1] V. de la Rubia, U. Razafison, and Y. Maday, "Reliable fast frequency sweep for microwave devices via the reduced-basis method," *IEEE Trans. Microw. Theory Techn.*, vol. 57, no. 12, pp. 2923–2937, Dec. 2009.

[2] Z. Bai, "Krylov subspace techniques for reduced-order modeling of large-scale dynamical systems," *Appl. Numer. Math.*, vol. 43, no. 1, pp. 9–44, Oct. 2002.

[3] A. Schultschik, O. Farle, and R. Dyczij-Edlinger, "An adaptive multipoint fast frequency sweep for large-scale finite element models," *IEEE Trans. Magn.*, vol. 45, no. 3, pp. 1108–1111, Mar. 2009.

[4] M. Rewieński, A. Lamecki, and M. Mrozowski, "Greedy multipoint model-order reduction technique for fast computation of scattering parameters of electromagnetic systems," *IEEE Trans. Microw. Theory Techn.*, vol. 64, no. 6, pp. 1681–1693, June 2016.

[5] A. Chatterjee, "An introduction to the proper orthogonal decomposition," *Current science*, vol. 78, no. 7, pp. 808–817, Apr. 2000.

[6] L. Feng, J. G. Korvink, and P. Benner, "A fully adaptive scheme for model order reduction based on moment matching," *IEEE Trans. Compon. Packag. Manuf. Technol.*, vol. 5, no. 12, pp. 1872–1884, Dec. 2015.

[7] V. de la Rubia and J. Zapata, "Microwave circuit design by means of direct decomposition in the finite-element method," *IEEE Trans. Microw. Theory Techn.*, vol. 55, no. 7, pp. 1520–1530, Jul. 2007.

[8] A. C. Cangellaris, "Electromagnetic macro-modeling: An overview of current successes and future opportunities," in *Computational Electromagnetics Int. Workshop (CEM)*, 2011, pp. 1–6.

[9] H. Wu and A. C. Cangellaris, "Krylov model order reduction of finite element approximations of electromagnetic devices with frequency-dependent material properties," *Int. J. Numer. Model.*, vol. 20, no. 5, pp. 217–235, 2007.

[10] B. Denecker, F. Olyslager, L. Knockaert, and D. De Zutter, "Automatic generation of subdomain models in 2D FDTD using reduced order modeling," *IEEE Microw. Guided Wave Lett.*, vol. 10, no. 8, pp. 301–303, Aug. 2000.

[11] L. Kulas and M. Mrozowski, "Reduced-order models in FDTD," *IEEE Microw. Compon. Lett.*, vol. 11, no. 10, pp. 422–424, Oct. 2001.

[12] Y. Zhu and A. C. Cangellaris, "Macro-elements for efficient FEM simulation of small geometric features in waveguide components," *IEEE Trans. Microw. Theory Techn.*, vol. 48, no. 12, pp. 2254–2260, Dec. 2000.

[13] G. Fotyga, M. Rewienski, and M. Mrozowski, "Wideband macromodels in finite element method," *IEEE Microw. Compon. Lett.*, vol. 25, no. 12, pp. 766–768, Dec. 2015.

[14] X. Zhang, F. Bekmambetova, and P. Triverio, "A stable FDTD method with embedded reduced-order models," *IEEE Trans. Antennas Propag.*, vol. 66, no. 2, pp. 827–837, Feb. 2018.

[15] A. Zadehgol, "An impedance transfer function formulation for reduced-order macromodels of subgridded regions in FDTD," *IEEE Trans. Antennas Propag.*, vol. 65, no. 1, pp. 401–404, Jan. 2017.

[16] Ł. Kulas and M. Mrozowski, "Multilevel model order reduction," *IEEE Microw. Compon. Lett.*, vol. 14, no. 4, pp. 165–167, Apr. 2004.

[17] G. Fotyga, K. Nyka, and M. Mrozowski, "Multilevel model order reduction with generalized compression of boundaries for 3-D FEM electromagnetic analysis," *Prog. Electromagn. Res.*, vol. 139, pp. 743–759, 2013.

[18] M. W. Hess, S. Grundel, and P. Benner, "Estimating the inf-sup constant in reduced basis methods for time-harmonic Maxwell's equations," *IEEE Trans. Microw. Theory Techn.*, vol. 63, no. 11, pp. 3549–3557, Nov. 2015.

[19] M. Rewienski, A. Lamecki, and M. Mrozowski, "A goal-oriented error estimator for reduced basis method modeling of microwave devices," *IEEE Microw. Compon. Lett.*, vol. 25, no. 4, pp. 208–210, Apr. 2015.

[20] Y. Konkel, O. Farle, A. Sommer, S. Burgard, and R. Dyczij-Edlinger, "A posteriori error bounds for Krylov-based fast frequency sweeps of finite-element systems," *IEEE Trans. Magn.*, vol. 50, no. 2, pp. 441–444, Feb. 2014.

[21] W. Wang, G. N. Paraschos, and M. N. Vouvakis, "Fast frequency sweep of FEM models via the balanced truncation proper orthogonal decomposition," *IEEE Trans. Antennas Propag.*, vol. 59, no. 11, pp. 4142–4154, Nov. 2011.

[22] A. Sommer, O. Farle, and R. Dyczij-Edlinger, "A new method for accurate and efficient residual computation in adaptive model-order reduction," *IEEE Trans. Magn.*, vol. 51, no. 3, pp. 1–4, Mar. 2015.

[23] P. Benner, S. Gugercin, and K. Willcox, "A survey of projection-based model reduction methods for parametric dynamical systems," *SIAM review*, vol. 57, no. 4, pp. 483–531, 2015.

[24] M. Hess and P. Benner, "Fast evaluation of time harmonic Maxwell's equations using the reduced basis method," *IEEE Trans. Microw. Theory Techn.*, vol. 61, no. 6, pp. 2265–2274, Jun. 2013.

[25] M. K. Sampath, A. Dounavis, and R. Khazaka, "Parameterized model order reduction techniques for FEM based full wave analysis," *IEEE Trans. Adv. Packag.*, vol. 32, no. 1, pp. 2–12, Feb. 2009.

[26] S. Burgard, O. Farle, and R. Dyczij-Edlinger, "A novel parametric model order reduction approach with applications to geometrically parameterized microwave devices," *COMPEL: Int. J. Comput. Math. Elect. Electron. Eng.*, vol. 32, no. 5, pp. 1525–1538, 2013.

[27] S. Burgard, O. Farle, D. Klis, and R. Dyczij-Edlinger, "Order-reduction of fields-level models with affine and non-affine parameters by interpolation of subspaces," *IFAC-PapersOnLine*, vol. 48, no. 1, pp. 170–175, 2015.

[28] S. Burgard, O. Farle, and R. Dyczij-Edlinger, "An h-adaptive sub-domain framework for parametric order reduction," *IEEE Trans. Magn.*, vol. 51, no. 3, pp. 1–4, Mar. 2015.

[29] R. Dyczij-Edlinger and O. Farle, "Finite element analysis of linear boundary value problems with geometrical parameters," *COMPEL-Int. J. Comput. Math. Elect. Electron. Eng.*, vol. 28, no. 4, pp. 779–794, 2009.

[30] S. Brandl and R. Dyczij-Edlinger, "Parametric model-order reduction for accelerating the gradient-based optimization of microwave structures using finite-elements," *IFAC-PapersOnLine*, vol. 51, no. 2, pp. 190–195, 2018.

[31] A. Lamecki, "A mesh deformation technique based on solid mechanics for parametric analysis of high-frequency devices with 3-D FEM," *IEEE Trans. Microw. Theory Techn.*, vol. 64, no. 11, pp. 3400–3408, Nov. 2016.

[32] V. de la Rubia, A. Lamecki, and M. Mrozowski, "Geometry parametric model order reduction with randomly generated projection bases," in *Numerical Electromagnetic and Multiphysics Modeling and Optimization (NEMO), 2016 IEEE MTT-S International Conference on*. IEEE, 2016, pp. 1–2.

[33] M. Czarniewska, G. Fotyga, and M. Mrozowski, "Local mesh morphing technique for parametrized macromodels in the finite element method," in *Proc. Int. Appl. Comput. Electromagn. Soc. Symp. - Italy (ACES)*, Mar. 2017, pp. 1–2.

[34] M. Czarniewska, G. Fotyga, A. Lamecki, and M. Mrozowski, "Parametrized local reduced-order models with compressed projection basis for fast parameter-dependent finite-element analysis," *IEEE Trans. Microw. Theory Techn.*, vol. 66, no. 8, pp. 3656–3667, Aug. 2018.

[35] G. Fotyga, K. Nyka, and M. Mrozowski, "Automatic reduction order selection for finite-element macromodels," *IEEE Microw. Compon. Lett.*, vol. 28, no. 4, pp. 278–280, Apr. 2017.

[36] ——, "Efficient model order reduction for FEM analysis of waveguide structures and resonators," *Prog. Electromagn. Res.*, vol. 127, pp. 277–295, 2012.

[37] L. Szydlowski and M. Mrozowski, "A self-equalized waveguide filter with frequency-dependent (resonant) couplings," *IEEE Microw. Compon. Lett.*, vol. 24, no. 11, pp. 769–771, Nov. 2014.

[38] R.-C. Li, "Matrix perturbation theory," in *Handbook of linear algebra*, L. Hogben, Ed. Chapman & Hall/CRC, 2007, pp. 15.9–15.11.